Atmósfera (1994), **7**, *pp. 221-240*

A sea breeze rainfall model

MARIANO A. ESTOQUE

Department of Meteorology and Oceanography, University of the Philippines, Diliman, Quezon City, Philippines

SHIRLEY V. ALMAZAN and JOSEFA C. MONDARES

Philippine Atmospheric and Geophysical Services Administration, Quezon City, Philippines

(Manuscript received Jan. 22, 1993; accepted in final form Oct. 15, 1993)

RESUMEN

Se describe un modelo numérico para estudiar el desarrollo de la lluvia de brisa marina en la vecindad de una costa en línea recta. El modelo se basa en ecuaciones primitivas, dependientes del tiempo. El modelo es capaz de describir explícitamente la formación de lluvia y sus subsecuentes variaciones en el espacio y el tiempo.

La descripción se hace incorporando una ecuación de predicción para agua de lluvia, la cual es derivada de una parametrización de procesos microfísicos de nubes. Una prueba inicial del modelo se hizo simulando la lluvia de brisa marina para un caso de flujo no predominante durante la estación lluviosa en el trópico. En general la simulación reproduce las características observadas de la lluvia de brisa marina. Se investiga la sensibilidad del modelo a las parametrizaciones microfísicas en las nubes, de las constantes asociadas con autoconversión y aumento por medio de experimentos numéricos. Los experimentos muestran que la lluvia es relativamente insensible a las constantes de autoconversión del modelo, pero muy sensible a la constante de acrecentamiento.

ABSTRACT

A numerical model for studying the development of sea breeze rainfall in the vicinity of a straight coastline is described. The model is based on the time-dependent primitive equations. The model is able to describe explicitly the formation of rain and its subsequent space and time variations. The description is done by incorporating a prediction equation for rain water which is derived through a parameterization of cloud microphysical processes. An initial test of the model is done by simulating the sea breeze rainfall for a case of no prevailing flow during the rainy season in the tropics. In general, the simulation reproduces the observed characteristics of sea breeze rainfall. The sensitivity of the model to the cloud microphysical parameterization constants associated with autoconversion and accretion is investigated by means of numerical experiments. The experiments show that the rainfall is relatively insensitive to the autoconversion model constants but quite sensitive to the accretion constant.

1. Introduction

The sea breeze, a circulation which is generated by the differential heating between land and the sea, is an important weather phenomenon in the tropics. The circulation is generally characterized by ascending air over land and descending air over the sea. The ascending motions are frequently associated with a band of convective clouds and rainfall. Sea breeze rainfall is a substantial percentage of the total rainfall in many tropical regions. According to Burpee and Lahiff (1984), the average sea breeze rainfall over the Florida Peninsula for highly–disturbed (synoptically) days is about 3.4 cm/day.

There are large variations in the intensity, duration, as well as the time and place of occurrence of sea breeze rainfall. The large variations must be due to corresponding variations in the large scale prevailing flow. When the synoptic conditions are characterized by a relatively unstable and moist air mass in a weak prevailing flow, sea breezes produce heavy rainfall. An onshore (sea to land) prevailing flow tends to produce a less intense rainfall which occurs relatively far from the shoreline. On the other hand, an offshore (land to sea) prvailing flow generally produces a more intense rainfall which occurs near the coastline. The configuration of the coastline and the existence of sloping terrain near the coast are also important factors in determining the characteristics of sea breeze rainfall. For example, mountain slopes tend to enhance the rainfall due to the coupling between sea breeze and upslope winds during the daytime.

Sea breeze rainfall normally occurs initially in the early afternoon, a short distance inland from the coastline. In general, the rain area subsequently moves progressively inland until it dissipates at night. However, under certain conditions, the rain tends to move back toward the coast late in the afternoon and lines of showers may develop near the beach at night. This appears to be common feature of sea breeze rainfall near Puerto Armuelles (Panama) according to Crow and Cobb (1962). This strange behavior of the sea breeze rainfall is the result of an unusual combination of the effects of topography and large scale prevailing conditions.

The objective of this paper is to describe the initial version of a model which may be used to study the interesting characteristics of sea breeze rainfall described above. The model predicts rainfall explicitly through a parameterization of cloud microphysical processes. An example of an integration of the model is presented. In addition, the sensitivity of the model to model constants relating to the rainfall parameterization is studied by means of numerical experiments.

2. Basic model equations

The present model is essentially an extension of previous models which have been described by Estoque and Bhumralkar (1969), Bhumralkar (1973) and Estoque *et al.* (1976). It is a primitive equation, time–dependent and two–dimensional (vertical $x - z$ cross–section) model. Here, x is the horizontal coordinate normal to the coastline while z is the vertical coordinate. The two–dimensionality limits the application of the model to sea breezes which are generated by straight coastlines. In order to incorporate the effects of topography conveniently in future applications, we have replaced the z coordinate with the so–called sigma (σ) coordinate. The transformation from z to σ is given by the expression:

$$\sigma = \frac{z - h}{H - h} \tag{1}$$

where h is the horizontally–varying height of the terrain while H is the upper boundary of the physical model. In applications of the model, H should be approximately equal to the height of the tropopause.

In order to incorporate the prediction of rainfall, we have included a parameterization of cloud microphysical processes based on the suggestions of Kessler (1969). Since turbulent mixing in the lowest layer of the atmosphere is an important process, we have also included a parameterization of this process. Details concerning both of these parameterizations are described in the next section.

The fundamental set of equations of the model consists of eight equations. Five of these are prediction equations while the remaining three are diagnostic equations. Corresponding to these eight equations are eight unknown variables. The five variables which are predicted directly by using the prediction equation are:

u - horizontal velocity component normal to the shoreline

v - horizontal velocity component parallel to the shoreline

Θ - potential temperature

Q_r - mixing ratio of rain water

Q - mixing ratio of water vapor plus cloud water

The three variables which are diagnosed from the above predicted variables are:

φ - Exner's function of pressure (see below)

σ - vertical velocity in the coordinate system

Q_c - mixing ratio of cloud water

The five prediction equations of the model are as follows:

$$\frac{\partial u}{\partial t} = -u\frac{\partial u}{\partial x} - \sigma\frac{\partial u}{\partial \sigma} + fv - C_p\Theta\frac{\partial}{\partial x}\left[\frac{P}{P_o}\right]^k - g(1-\sigma)\frac{\partial h}{\partial x}$$

$$+\frac{1}{(H-h)^2}\frac{\partial}{\partial \sigma}\left[K_z\frac{\partial u}{\partial \sigma}\right] + K_x\left[\frac{\partial^2 u}{\partial x^2} - \frac{(1-\sigma)}{(H-h)^2}\left[\frac{\partial^2 u}{\partial \sigma \partial x}\right]\frac{\partial h}{\partial x}\right] \tag{2}$$

$$\frac{\partial v}{\partial t} = -u\frac{\partial v}{\partial x} - \dot{\sigma}\frac{\partial v}{\partial \sigma} + f(u_g - u) + \frac{1}{(H-h)^2}\frac{\partial}{\partial \sigma}\left[K_z\frac{\partial v}{\partial \sigma}\right]$$

$$+K_x\left[\frac{\partial^2 v}{\partial x^2} - \frac{1-\sigma}{H-h}\left[\frac{\partial^2 v}{\partial \sigma \partial x}\right]\frac{\partial h}{\partial x}\right] \tag{3}$$

$$\frac{\partial \Theta}{\partial t} = -u\frac{\partial \Theta}{\partial x} - \dot{\sigma}\frac{\partial \Theta}{\partial \sigma} + \frac{1}{(H-h)^2}\frac{\partial}{\partial \sigma}\left[K_x\frac{\partial \Theta}{\partial \sigma}\right]$$

$$+K_x\left[\frac{\partial^2 \Theta}{\partial x^2} - \frac{1-\sigma}{H-h}\left[\frac{\partial^2 \Theta}{\partial \sigma \partial x}\right]\frac{\partial h}{\partial x}\right] + \frac{\Theta}{C_pT}(S_1 + S_2) \tag{4}$$

$$\frac{\partial Q}{\partial t} = -u\frac{\partial Q}{\partial x} - \dot{\sigma}\frac{\partial Q}{\partial \sigma} + \frac{1}{(H-h)^2}\frac{\partial}{\partial \sigma}\left[K_z\frac{\partial Q}{\partial \sigma}\right]$$

$$+K_x\left[\frac{\partial^2 Q}{\partial x^2} - \frac{1-\sigma}{H-h}\frac{\partial^2 Q}{\partial \sigma \partial x}\frac{\partial h}{\partial x}\right]$$

$$+\frac{1}{\rho_s}[-AUCON(Q \rightarrow Q_r) - ACR(Q \rightarrow Q_r) + EVAP(Q_r \rightarrow Q)] \tag{5}$$

$$\frac{\partial Q_r}{\partial t} = -u\frac{\partial Q_r}{\partial x} - \dot{\sigma}\frac{\partial Q_r}{\partial \sigma} - \frac{1}{\rho_s}\frac{1}{(H-h)}\frac{\partial}{\partial \sigma}(\rho_s V_r Q_r)$$

$$+\frac{1}{\rho_s}[AUCON(Q \rightarrow Q_r) + ACR(Q \rightarrow Q_r) - EVAP(Q_r \rightarrow Q)] \tag{6}$$

$$\frac{\partial \varphi}{\partial \sigma} = -\frac{g}{\Theta}(H-h) \tag{7}$$

where

$$\varphi = C_p\left[\frac{P}{P_o}\right]^k; \quad k = R/C_p \tag{8}$$

$$\frac{\partial \rho_s \dot{\sigma}}{\partial \sigma} + \frac{\partial \rho_s u}{\partial x} = 0 \tag{9}$$

Eqs. (2) and (3) are the momentum equations along the horizontal coordinates normal and parallel to the coastline, respectively. Eq. (4) is the thermodynamic energy equation, Eq. (5) is the conservation equation for water in vapor plus cloud water, Eq. (6) is the conservation equation for rainwater, Eq. (7) is the hydrostatic equation and Eq. (8) is the definition for φ. Finally, Eq. (9) is an anelastic version of the continuity equation.

The notation in the equation follows, in general, the customary convention in meteorology. The quantity, ρ_s, is the density for the standard atmosphere which is a function of height. The nonconservative terms as well as the diffusion terms in Eqs. (2) to (6) are described below.

3. Incorporation of nonconservative processes

In this section, we will describe the formulation of the terms in Eqs. (2) to (6) which involve sinks and sources, including the parameterization of cloud microphysical processes and turbulent fluxes. As mentioned in the previous section, the cloud microphysical processes are parameterized with the aid of the formulation by Kessler (1969). According to his formulation, cloud droplets form into raindrops through two processes: autoconversion and accretion (denoted as *AUCON* and *ACR* in the prediction equation). The term *AUCON* is given by

$$AUCON = K_1[\rho_s(Q - Q_s) - K_2],$$

where K_1 and K_2 are empirical constants and

$$K_1 \begin{cases} > 0 & \text{for } \rho_s(Q - Q_s) > K_2 \\ = 0 & \text{for } \rho_s(Q - Q_s) < K_2 \end{cases}$$

K_2 is a threshold value which has to be exceeded by $\rho_s(Q - Q_s)$ in order to initiate the autoconversion. The saturation mixing ratio is represented by Q_s, while ρ_s stands for the density of air. The term ACR is represented by

$$ACR = C_e K_3 \rho_s (Q - Q_s)(\rho_s Q_r \times 10^6)^{.875},$$

where C_e is the collection efficiency and

$$K_3 \begin{cases} > 0 & \text{for } Q > Q_s \text{ and } Q_r > 0 \\ = 0 & \text{for } Q < Q_s \end{cases}$$

Q_s is the saturation mixing ratio. The evaporation of raindrops ($EVAP$) is given by,

where $$EVAP = K_4 \rho_s [Q_s - Q](\rho_s Q_r 10^6]^{0.65},$$

$$K_4 \begin{cases} > 0 & \text{for } Q < Q_s \text{ and } Q_r > 0 \\ = 0 & \text{for } Q > Q_s \end{cases}$$

The quantities S_1 and S_2 in Eq. (4) represent heating by condensation and cooling due to evaporation of water droplets as a result of vertical motions and horizontal mixing. The expressions for these quantities are:

$$S_1 = K_5 \left[-L \frac{dQ_s}{dt} \right]$$

where

$$K_5 = \begin{cases} 1 & \text{for} Q \geq Q_s \\ 0 & \text{for} Q < Q_s, \end{cases}$$

and

$$\frac{\partial Q_s}{\partial t} = -\frac{g}{R} \left[\frac{\varepsilon L - C_p \overline{T}}{C_p \overline{T}^2 + \frac{L^2 Q_s}{R_v}} \right] Q_s \omega,$$

$$S_2 = -K_6 [EVAP(Q_r \rightarrow Q)],$$

where

$$K_6 \begin{cases} = 0 & \text{for } Q \geq Q_s \\ = 1 & \text{for } Q < Q_s \end{cases}$$

where K_6 is a switching constant which is equal to zero or one if the atmosphere is unsaturated or saturated, respectively; K_x represents the horizontal diffusion coefficient.

The terminal velocity (V_r) in Eq. (6) is computed by the method described by Murray and Koenig (1972). By this method, the velocity is parameterized as follows:

$$V_r = -38.3 \times N_o^{-1/8} (\rho_s Q_r \times 10^6)^{1/8}$$

The vertical fluxes of momentum, heat and moisture in the boundary layer are quantities which are needed in the integrations of Eqs. (2) to (5). These are computed in terms of the velocity (friction) scale U_*, the potential temperature scale Θ_*, and the humidity scale q_*. In terms of these scaled quantities the fluxes are U_*^2, $U_*\Theta_*$, $U_* q_*$. The values of U_*, Θ_* and q_* are computed from the vertical profiles of wind speed, potential temperature and mixing ratio with the aid of similarity theory. The computation uses these profiles in conjunction with values of u, v, and q at two levels, at the Earth's surface and at the first prediction level above the surface. At layers above the prediction level, the fluxes are expressed in terms of a diffusion coefficient which is given by:

$$K_z = \begin{cases} l^2 \frac{\partial u}{\partial z}(1 - \alpha S) & \text{for } \frac{\partial \Theta}{\partial z} < 0 \\ l^2 \frac{\partial u}{\partial z}(1 + \alpha S)^{-1} & \text{for } \frac{\partial \Theta}{\partial z} > 0 \end{cases}$$

where

$$l = k_o(z + z_o)\left[1 + \frac{f(z + z_o)k_o}{27 \times 10^{-5}\, U(z = H)}\right],$$

and

$$S = \frac{(gl)^{1/2}}{\Theta} \frac{\partial \Theta / \partial z}{\left| \frac{\partial u}{\partial z} \right|},$$

U is the horizontal wind speed and α is an empirical constant with an assumed value of 18, based on observations.

4. Computational aspects and boundary conditions

The domain of computation (Fig. 1) is a rectangular (vertical) section in the $x - \sigma$ coordinate system. The bottom of the rectangle is located at $\sigma = 0$ while the top is located at $\sigma = 1$; over flat terrain $\sigma = 0$ and $\sigma = 1$ correspond to sea level and to the 12 km level, respectively. The horizontal dimension of the domain is 1000 km with the coastline at the midpoint ($x = 0$). There are 17 gridpoints along the vertical and 31 gridpoints along the horizontal. The gridpoint spacing is variable along both horizontal and vertical directions with small grid distances near the Earth's surface and near the coastline. In these regions, the gradients of the meteorological quantities are expected to be strong. The actual positions of the gridpoints are shown in Table 1.

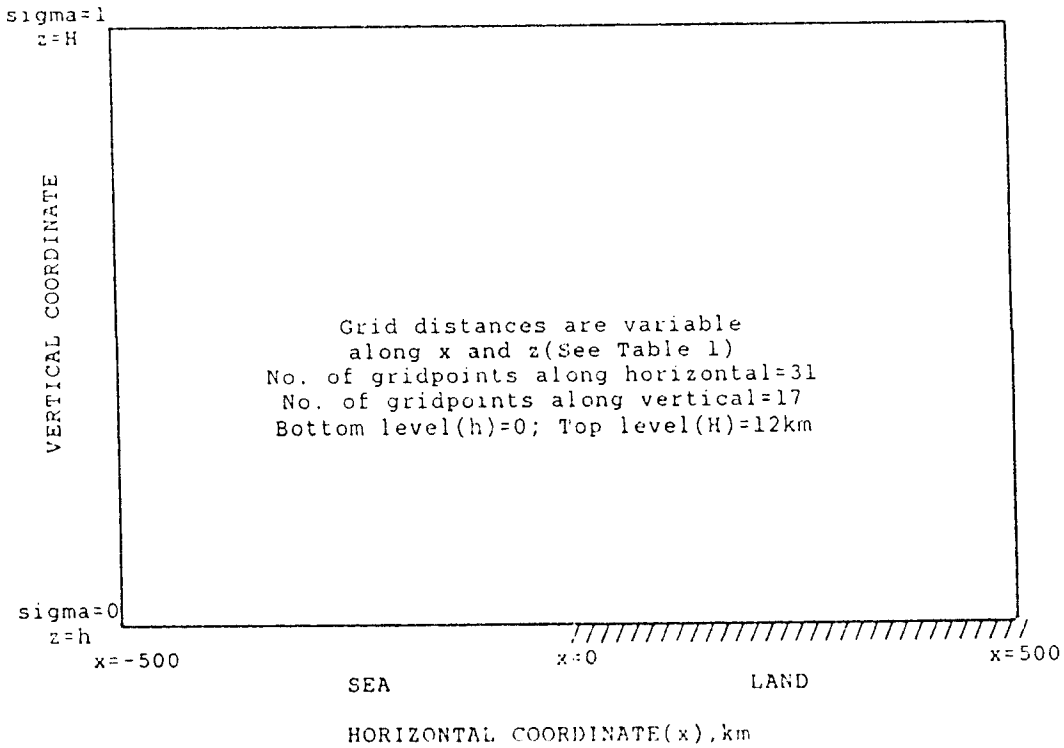

Fig. 1. Domain of computation.

Table 1. Coordinates of gridpoints along the vertical and the horizontal (x) directions. The coastline is located at $x = 0$; positive values of x correspond to land.

J	z(meters)	I	x(km)	I	x(km)
1	0	1	-500	18	10
2	10	2	-390	19	16
3	25	3	-310	20	24
4	225	4	-250	21	35
5	425	5	-200	22	50
6	650	6	-155	23	68
7	900	7	-120	24	90
8	1200	8	-90	25	120
9	1550	9	-68	26	155
10	1950	10	-50	27	200
11	2450	11	-35	28	250
12	3100	12	-24	29	310
13	3900	13	-16	30	390
14	4900	14	-10	31	500
15	6300	15	-5		
16	8500	16	0		
17	12000	17	5		

The finite differencing is forward in time and upstream in the space derivatives of the advective terms. The values of other space derivatives at any particular point, e.g., pressure gradient term, are approximated with the aid of a Taylor Series expansion: the expansion uses the value at the gridpoint and the other two adjacent values at each side of the gridpoint. The important boundary conditions for the solution of the equations are as follows:

Lateral boundaries: At inflow points, the boundary values are held constant during the time step. At outflow points, the values are predicted using the finite differencing described above. After the calculation of the boundary values, a sponge is applied by using the method suggested by Lorenzetti and Wang (1986) in order to minimize boundary–generated noise.

Upper boundary ($\sigma = 1$ or $z = H$). The predicted variables (u, v, Q, Θ and Q_T) are held constant, equal to the corresponding values of the prevailing flow. The value of σ is set equal to zero. The value of $\varphi(\equiv \varphi_H)$ is specified according to a method described by Estoque *et al.* (1976).

Lower boundary conditions ($\sigma = 0$ or $z = h$): Both horizontal velocity components (u, v) and the vertical velocity (σ) are set equal to zero. The value of Q_T is set equal to its value at the first prediction level above the Earth's suface. The value of Θ is specified as:

$$\Theta = \begin{cases} \Theta_{sea} + 10\sin(2\pi t/24); & \text{for the land surface and} \\ \Theta_{sea}; & \text{for the sea surface.} \end{cases}$$

where t is the number of hours after midnight. Finally, the value of Q is computed from the surface temperature and a prescribed value of the relative humidity, which is 100% at the sea surface and 50% at the land surface.

5. An example of a simulation

In order to assess the performance of the model, we integrated the model equations for a case with no prevailing flow over flat terrain. The developing, the mature, and early dissipating stages

Table 2. Vertical distributions of potential temperature and relative humidity of the prevailing flow.

Height (m)	Potential Temperature, °K	R. H.,%
0	300	90
10	300	90
25	300	90
225	300	90
425	300	90
650	300	90
900	301	90
1200	302	90
1550	303	85
1950	304	85
2450	306	85
3100	310	85
3900	313	75
4900	317	75
6300	325	70
8500	335	65
12000	345	50

of the sea breeze rainfall system were simulated. The vertical distributions of temperature and relative humidity (Table 2) for the prevailing flow were based on an upper air sounding from Clark Air Force Base (Philippines) during the rainy season. The distributions correspond to a highly unstable (convectively) atmosphere. On the basis of these distributions, an undiluted air parcel which originates at the surface layers would arrive at the 500–mb level with a temperature excess of about 10°C over the environment. The value of the Coriolis parameter corresponds to that of 10°N latitude. The initial time for the integration was specified to be 0800 LCT. At this time, the land and the sea surface temperatures have the same value of 300°K. The initial values of the horizontal wind components (u, v) were assumed to be zero. The corresponding values of the potential temperature and the relative humidity are those shown in Table 2, and the respective profiles are illustrated in Figure 2. The mixing ratio for rain water (Q_r) was set equal to zero.

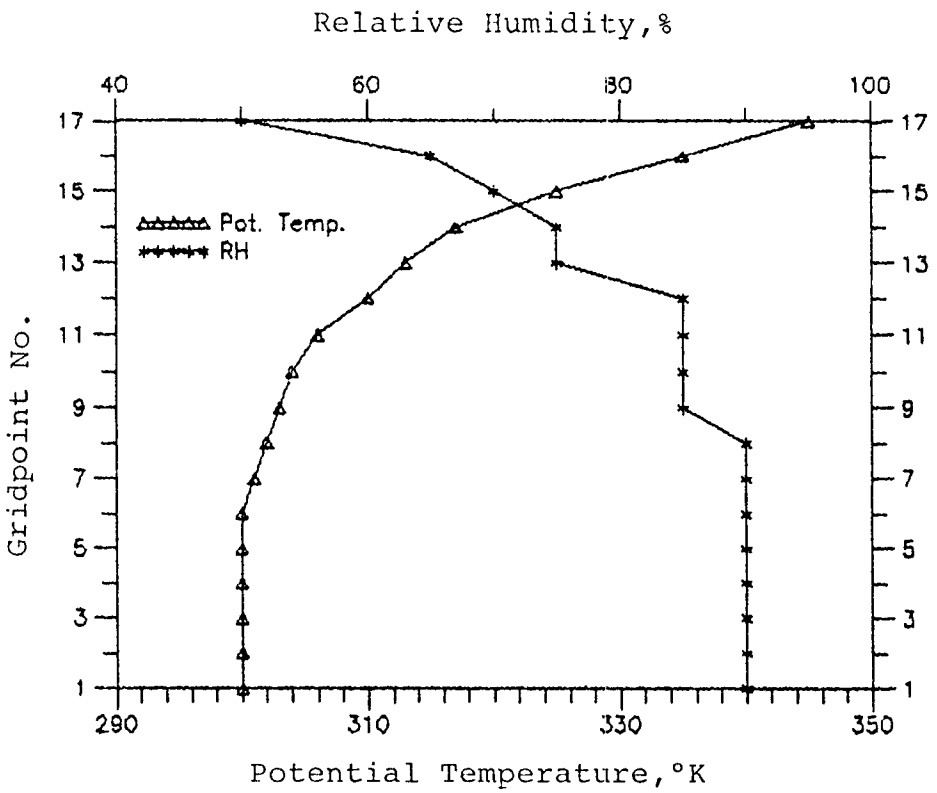

Fig. 2. Vertical profiles of potential temperature and relative humidity.

The evolution of the sea breeze circulation is shown in Figures 3 to 6. In these diagrams, note that the grid spacing is variable along the vertical and the horizontal directions. This is indicated by the distances along the coordinate axes. The vectors are drawn at each gridpoint on the basis of the computed values of u and ω components. In order to accentuate the vertical circulation, we multiplied the ω–component by 10 before plotting the vector. Looking at Figure 3, which represents the early stage of the sea breeze development at 1400 LCT, one can see a shallow onshore flow with a maximum speed of 5 m/sec found at lower levels some 10 to 16 km inland. The thickness of this onshore flow is about 500 meters. Overlying this shallow onshore flow, we see a much thicker but weaker return flow. The maximum speed of this return flow is about 2 m/sec. Figures 4 to 6 show the gradual intensification of the sea breeze circulation with time; the vertical as well as the horizontal dimensions of the onshore flow have correspondingly increased.

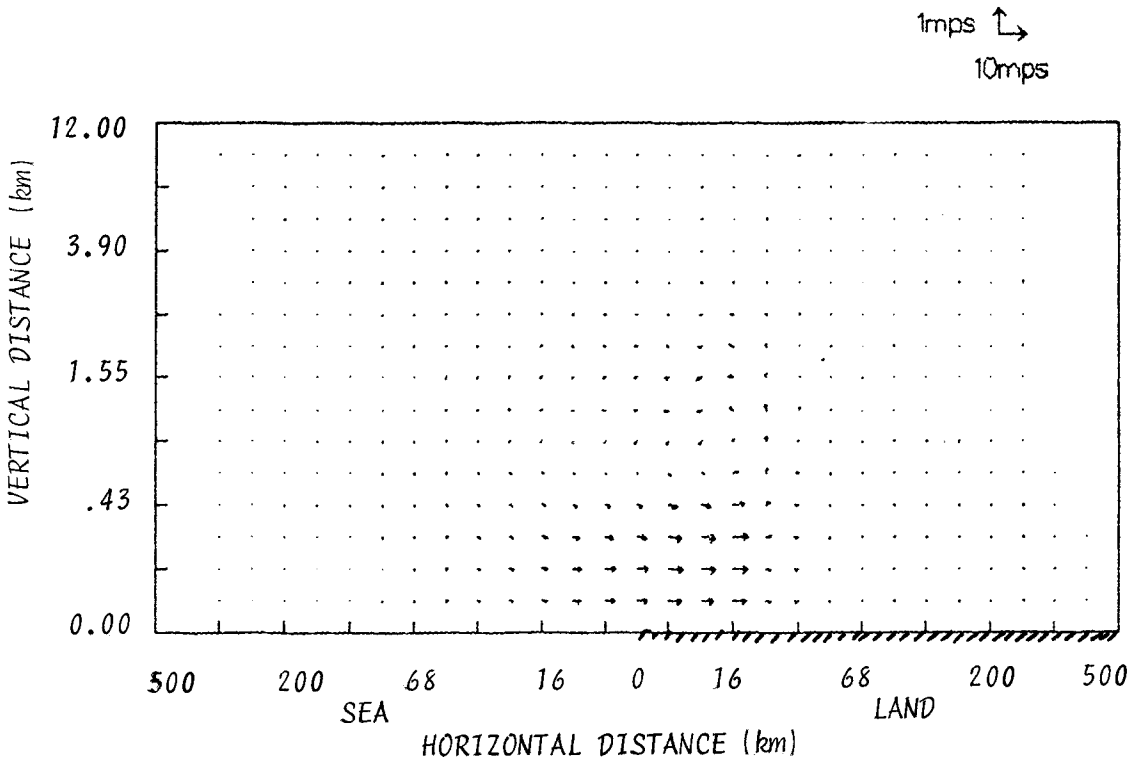

Fig. 3. Vertical circulation at 2 p. m. showing the early stages of development of the sea breeze.

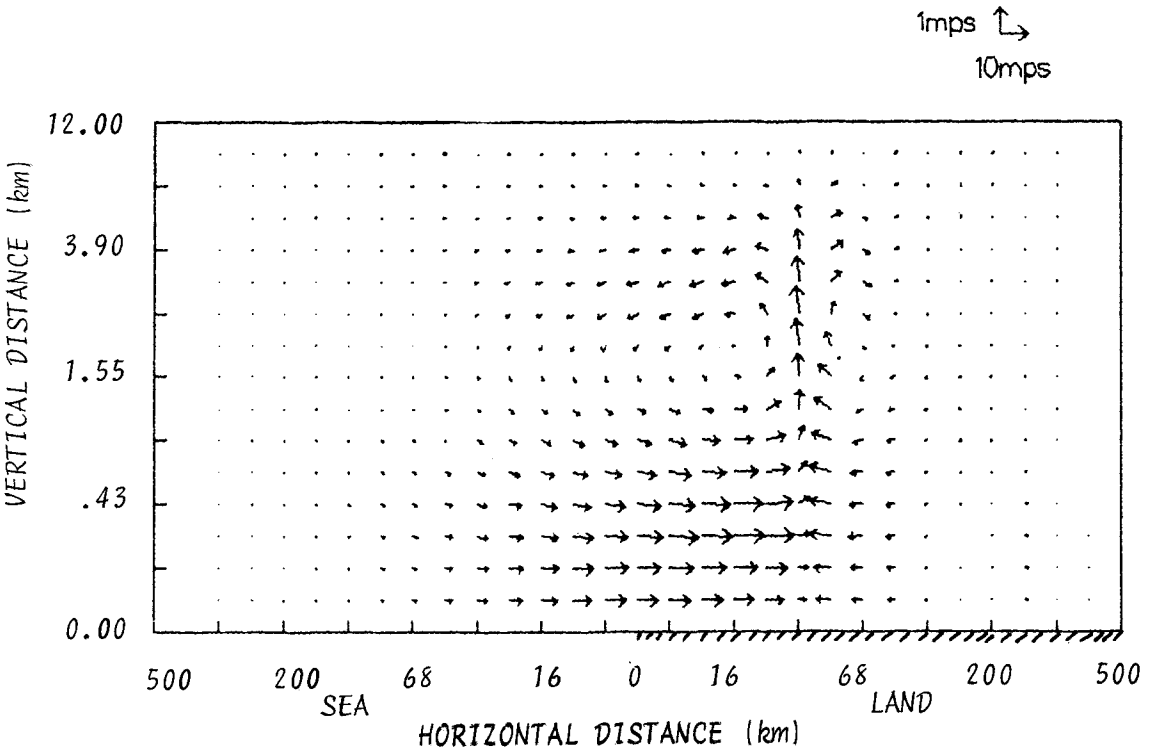

Fig. 4. The sea breeze circulation at 4 p. m. The maximum horizontal wind component in the diagram is about 11 m/sec.

Furthermore, the zone of maximum upward motion (the so–called sea breeze front) has moved continuously away from the coastline. At 1600 LCT, the sea breeze front has advanced to a location of about 35 km from the coastline. The maximum intensity of the sea breeze circulation is attained at 1800 LCT. At this time, the maximum horizontal wind component is about 13 m/sec while the corresponding vertical (upward) component is about 1.5 m/sec. The onshore flow has also thickened considerably to a height of about 2.5 km. Subsequently, the circulation progressively weakens. At 2200 LCT the maximum horizontal wind component is about 11 m/sec and the associated maximum upward velocity is 60 cm/sec.

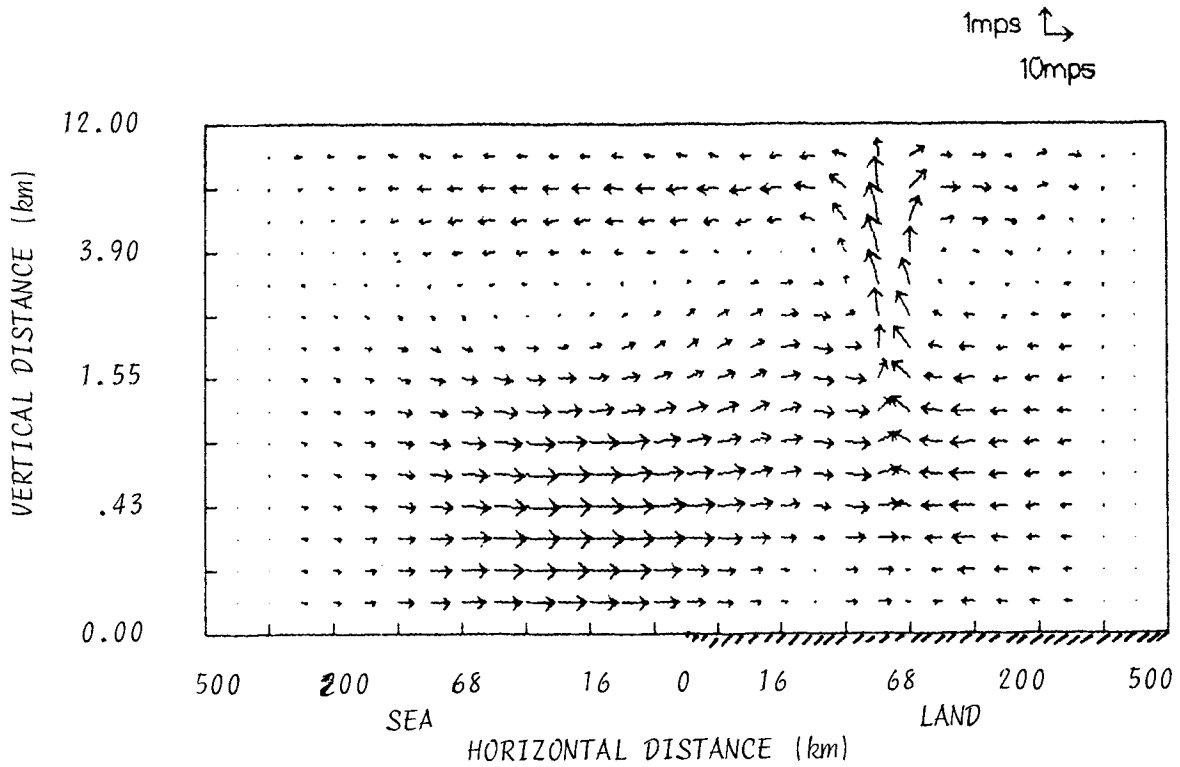

Fig. 5. The sea breeze circulation at 6 p. m. The maximum horizontal wind component in the diagram is about 15 m/sec and the vertical wind component is equal to about 132 cm/sec.

Next, we discussed the main emphasis of the study which is the modelling of the distribution of liquid water particularly the rainfall. Figure 7 shows the evolution of the cloud water as indicated by the quantity, $Q_{sup} \equiv Q - Q_s$ at the 1.2 km level. Note that if, Q_{sup} is positive, the value is equal to the cloud water content. On the other hand, a negative value indicates the value of the saturation deficit. Looking at Figure 7, one may see that the initial effect of the upward motions associated with the sea breeze is a slight decrease in the magnitude of the saturation deficit in the region of about 10 to 16 km inland away from the coastline at 1200 LCT. The initial sea breeze cloud at the 1.2 km level appears to form between 1200 LCT and 1400 LCT. At 1400 LCT, there is a cloud band between 16 to 24 km from the coastline. The cloud band moves steadily away from the coast reaching a distance of about 90 km at 2000 LCT. The average speed of movement of the band is about 10 km/hr. Note that there are generally large saturation deficits on each side of the cloud bands (shaded areas). These are due to the effect of descending motions.

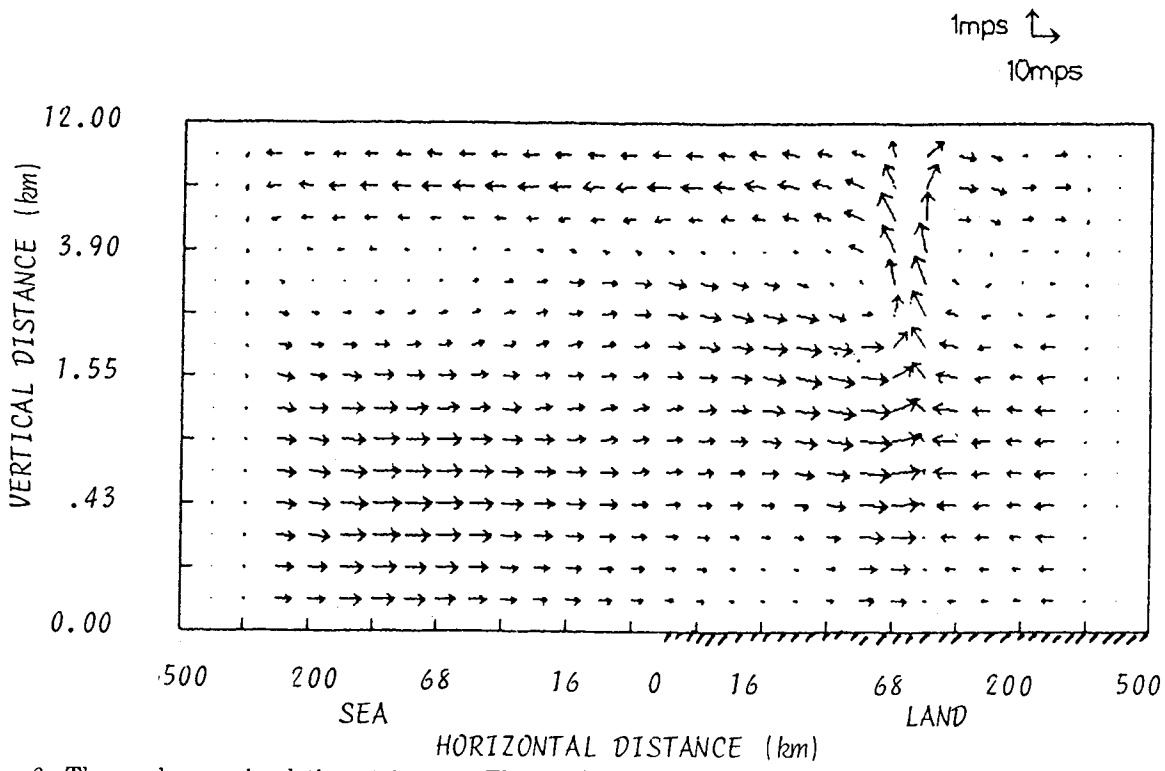

Fig. 6. The sea breeze circulation at 8 p. m. The maximum horizontal wind component in the diagram is about 11 m/sec and the vertical wind component is about 109 cm/sec.

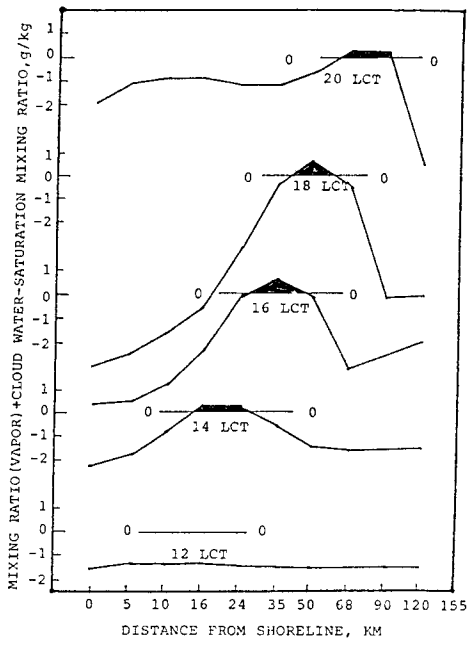

Fig. 7. The horizontal profiles of the mixing ratio of water vapor plus cloud water minus the saturation mixing ratio at the 1200 meter level. The shaded portions are cloudy regions.

The evolution of the water (water in cloud plus water in rain) cloud is shown in Figures 8 to 11. The diagrams show the isopleths of the total liquid water content, Q_c plus Q_r. Note that the smallest value of the isopleth shown in the figure is 0.1 gm of water per kg of air, implying that the computed water cloud outline is actually larger than what is shown in the diagrams. Looking at Figure 8, one can see that the water cloud at 1600 LCT, is located at about 35 km from the coastline. The cloud base and the cloud top are located at about 0.5 km and 4 km on the basis of the original grid data. The maximum liquid water content at this time is approximately 3.65 gm of water per kg of air. Two hours later (1800 LCT) the water cloud has increased not only in dimensions (horizontal and the vertical) but also in liquid water content. The shape of the water cloud resembles a cumulonimbus cloud with an anvil which extends towards the shoreline.

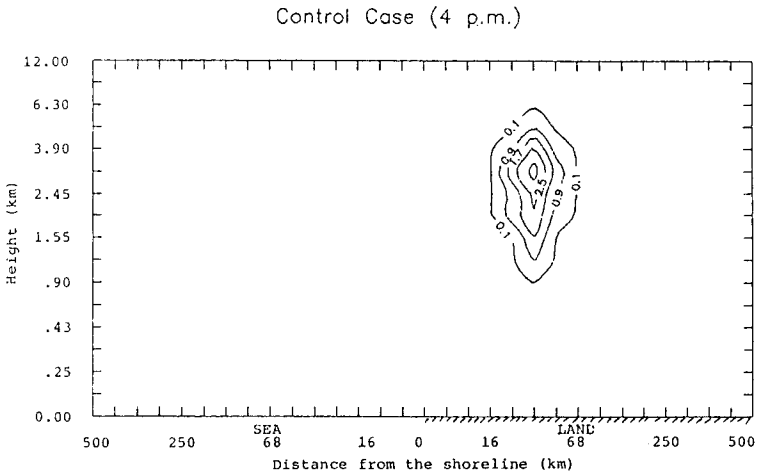

Fig. 8. The distribution of total liquid water content (g/kg) at 4 p. m. Contour interval equals 0.5 g/kg.

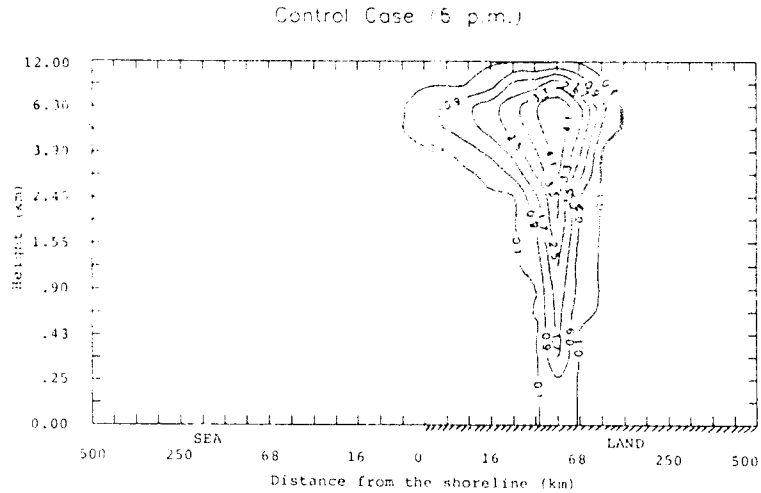

Fig. 9. The distribution of total liquid water content (g/kg) at 6 p. m. Contour interval equals 0.5 g/kg.

The shoreward extension of the upper portion of the cloud is mainly due to the advection by the return flow (Fig. 9) at upper levels. The maximum value of the liquid water content is about 5 gm of water per kg of air; this value is located at about an altitude of 6 km. Note also that, at this time, the water cloud (rain) has reached the ground. The maximum value at the ground is about 1.5 gm of water per kg of air. The liquid water content at this level consists only of rain

drops. Assuming a terminal velocity of 3 meters, we estimate the rainfall rate to be about 1.6 cm/hr. After 1800 LCT, there is a decrease in the values of the liquid water content. Four hours later (2200 LCT), the maximum values have decreased to about one half of the corresponding values at 1800 LCT. Note however, that the horizontal extent occupied by the water cloud at upper levels has increased considerably. Furthermore, the shape of the cloud indicates a greater extension of the anvil-like feature on its seaward side. This feature is a result of the continued horizontal advection of liquid water by the return flow of the sea breeze circulation at upper levels. A further decrease in the total liquid water content occurs subsequently. This decrease is due to the depletion of rainwater through the falling of raindrops as well as the absence of cloud water generation by ascending motions. At 0200 LCT (Fig. 11), one can see that only the upper part of the anvil remains while the lower part of the water cloud has practically disappeared. The shape of the cloud at this time is very similar to the conceptual model suggested by House *et al.* (1981) of a dissipating convective cloud near Borneo.

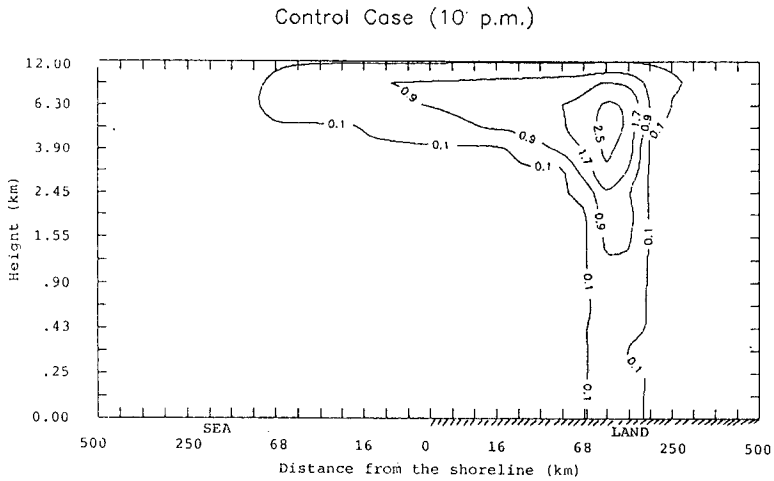

Fig. 10. The distribution of total liquid water content (g/kg) at 10 p. m. Contour interval equals 0.5 g/kg.

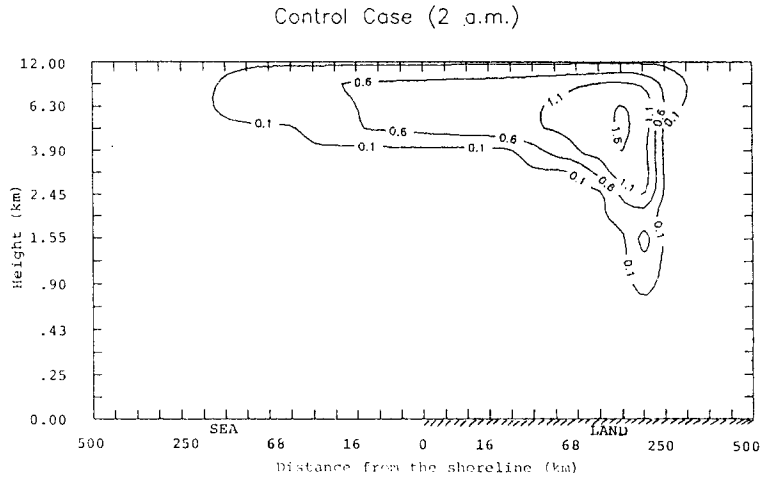

Fig. 11. The distribution of total liquid water content (g/kg) at 2 a. m. Contour interval equals 0.5 g/kg.

In summary, the initial version of the model is able to reproduce many of the important features of sea breeze rainfall. It has simulated the life cycle of the rain pattern, starting from its initial formation up to its early dissipating stage. In addition, it has also simulated the movement

of the rain pattern away from the shoreline during its lifetime. There are three unexpected characteristics of the simulated rainfall patterns; (1) the late occurrence of the rainfall, (2) the large distance of the rainfall band from the coastline and (3) the high rainfall intensity. All of these characteristics are presumably due to the use of a highly unstable atmosphere.

6. Sensitivity tests

In addition to the model simulation described above, we have also made several integrations for the purpose of determining the sensitivity of the model to some of the model constants. It will be noted that the main emphasis in the current modelling work is directed toward the simulation of rainfall. Hence, we have considered first the sensitivity with respect to the model constants which were used in connection with the cloud microphysical processes. In particular, the two processes which have been selected for the sensitivity tests are the autoconversion ($AUCON$) and the accretion (ACR) processes in Eqs. (5) to (6). The model constants in these processes are K_1, K_2 and K_3. The values of these constants which were used in the initial integration described above (defined as the control run) are based on Kessler's (1969) values. In order to determine the sensitivity of the rainfall to the value of any constant (say K_1), we made two additional integrations for comparison with the control run. In each of these integrations, we used a different value of K_1, however, the values of K_2 and K_3 were kept the same as the values in the control run. The same approach was used in determining the sensitivity of the model to different values of K_2 and K_3. The sensitivity test runs are summarized in Table 3.

Table 3. Integration runs for the sensitivity tests

Run No.	Value of Constants		
	Autoconversion Factor, K_1	Threshold Value, K_2	Collection Efficiency, K_3
1. (control)	1×10^{-4}	5×10^{-7}	1.0
2.	1×10^{-3}	5×10^{-7}	1.0
3.	1×10^{-5}	5×10^{-7}	1.0
4.	1×10^{-4}	0.0	1.0
5.	1×10^{-4}	5×10^{-6}	1.0
6.	1×10^{-4}	5×10^{-7}	0.1
7.	1×10^{-4}	5×10^{-7}	10.0

There are three sets of runs. The first set consists of Run No. 1 to No. 3; this set was used to determine the model sensitivity to the autoconversion factor (K_1). The other two sets (Nos. 1, 4 and 5) and (Nos. 1, 6 and 7), were used to determine the model sensitivity to the threshold value (K_2) and the collection efficiency (K_3), respectively. The results of these tests are shown graphically in Figures 12 to 14. Note that each figure consists of three diagrams, corresponding to three values of a particular microphysical model constant. Each diagram, in turn, consists of three rainfall intensity profiles (horizontal variation along the direction normal to the coastline) for three different instants of time: 1800 LCT, 2000 LCT and 2200 LCT. Note also that the middle diagram shows the rainfall intensity for the control run, corresponding to the simulation described in the previous section.

First we look at Figure 12 which shows the sensitivity of the rainfall intensity to different values of the autoconversion factor. It may be seen that the intensity is not very sensitive to the autoconversion factor. As the conversion factor increases a hundredfold, an increase of only about 15% in the intensity was noted. This relatively slight sensitivity is unexpected. The apparent explanation for this surprising result is as follows: If the autoconversion factor is low (high), less (more) cloud water is converted into rain water by autoconversion. Thus, more (less) liquid water remains in the form of cloud water. This condition results in more (less) rain water

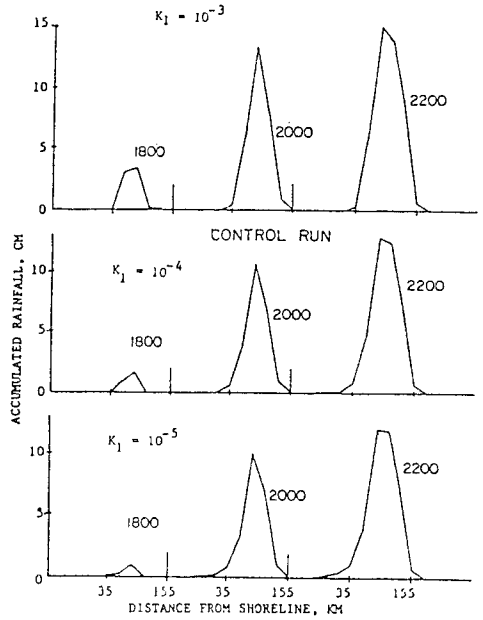

Fig. 12. The dependence of accumulated rainfall (cm) on the autoconversion factor (K_1). Left protion, 6 p. m.; middle portion, 8 p. m.; right portion, 10 p. m.

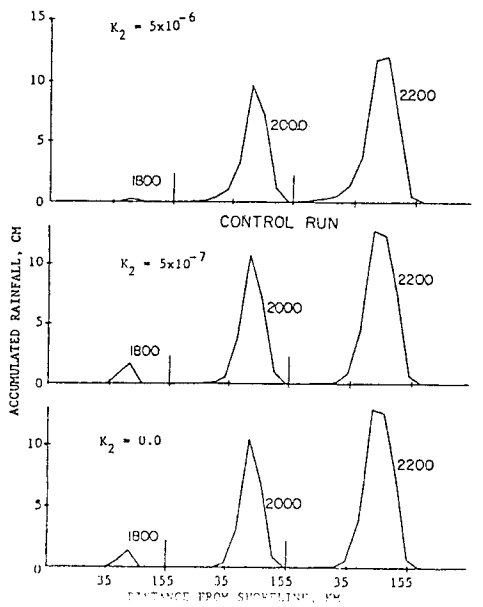

Fig. 13. The dependence of accumulated rainfall (cm) on the threshold value of cloud water (K_2). Left portion, 6 p. m.; middle portion, 8 p. m.; right portion, 10 p. m.

being produced by accretion because there is a greater (lesser) amount of cloud water for the raindrops to collect. In other words, the autoconversion and the accretion processes tend to compensate for one another. The overall result is to minimize the sensitivity of the model to change in the values of the autoconversion factor.

Next, we look at the sensitivity of the rainfall intensity to the threshold value of the cloud water in the autoconversion process (Fig. 13). Note that this value also tends to control the amount of cloud water which is converted into rainwater. The three values of the threshold values which were used are 0.0, 5×10^{-7} and 5×10^{-6} gm of water per cm^3. It may be seen that, as in the case of the autoconversion factor, the rainfall intensity is not very sensitive to different values of the threshold value. The explanation for this finding appears to be similar to the one described above for the autoconversion factor.

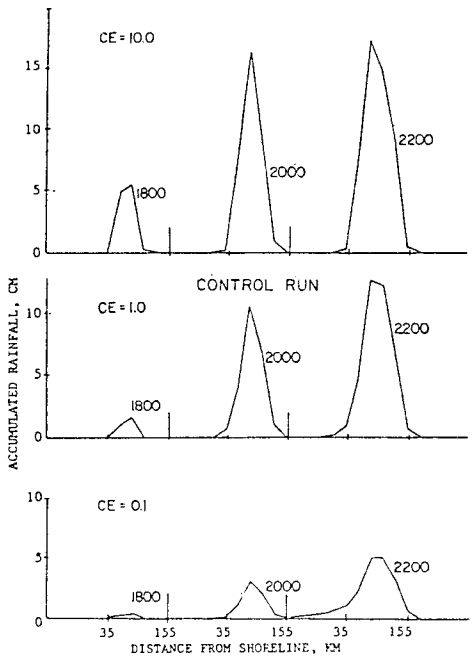

Fig. 14. The dependence of accumulated rainfall (cm) on the collection efficiency (C_{e_ϕ}). Left portion, 6 p. m.; middle portion, 8 p. m.; right portion, 10 p. m.

Finally, we look at the sensitivity of the model to the accretion process Figure 14. We see that the rainfall intensity is quite sensitive to the different values of the collection efficiency. As expected, larger values of the collection efficiency are associated with greater rainfall intensity. The model is sensitive especially at small values of the collection efficiency. For example, the tenfold increase of the value from 0.1 to 1.0 produces almost a threefold increase in the rainfall intensity. On the other hand, the tenfold increase of the value from 1.0 to 10.0 produces only about 30% in the rainfall intensity. The explanation for the much greater sensitivity to the collection efficiency as compared to the autoconversion factor and the threshold value is not readily apparent. This different behavior may be related to the fact that accretion is a nonlinear process in terms of cloud water and rainwater.

7. Concluding comments

In this paper, we have described a numerical model of sea breeze rainfall. An initial integration of the model has been made in order to simulate the sea breeze rainfall for a case with no prevailing flow during the rainy season. On the whole, the simulation is able to capture many features of the observed sea breeze rainfall such as, the initiation of the rainfall over land in the afternoon, its subsequent intensification as well as movement away from the shoreline, and its final dissipation late at night. The sensitivity of the simulated rainfall to several cloud microphysical model constants have been investigated. The investigation shows that the simulated rainfall intensity is relatively insensitive to the constants associated with the autoconversion process. On the other hand, the rainfall intensity is fairly sensitive to the accretion process model constant for collection efficiency.

Although the simulated sea breeze circulation and rainfall patterns are essentially correct, they revealed some surprising features.

Some of these are:

(a) the large horizontal extension of the sea breeze circulation over the sea,

(b) the unusually large thickness of the sea breeze (landward) flow during the fully-developed stage of the circulation,

(c) the large inland penetration by sea breeze,

(d) the high rainfall intensity and long rainfall duration lasting past midnight.

There are several possible reasons for these unusual features. One of these is the use of a simple sinusoidal surface temperature which is unaffected by the effects of cloud shading and rainfall reaching the ground. Another is the use of an unusually convectively unstable sounding for specifying the initial temperature and the specific humidity. The final explanation of these unusual features could be done with the aid of further improvements of the model in combination with actual sea breeze observations.

APPENDIX

List of symbols

$AUCON$	Autoconvertion
ACR	Accretion
C_e	collection efficiency
C_p	specific heat capacity of air at constant pressure
$EVAP$	evaporation
f	Coriolis parameter
g	acceleration due to gravity
H	height of grid domain, equal to 12 km
h	height of terrain
I	horizontal index in the grid domain
J	vertical index in the grid domain
k	R/c_p
k_o	Von Karman constant
K_x	horizontal diffusion coefficient
K_z	vertical diffusion coefficient
L	latent heat of evaporation
N_o	$= 10^7$ (intercept of Marshall-Palmer curve)

P_o	reference level pressure (1000 mb)
P	pressure
P_T	pressure at the top of the model
Q_o	mixing ratio of ground level
Q_v	mixing ratio of water vapor
Q_r	mixing ratio of rain water
Q_s	saturation mixing ratio
Q_c	mixing ratio of cloud water
Q_*	friction mixing ratio
R	gas constant of dry air
R_v	gas contant for vapor
S_1	latent heat release or consumed due to change of phase
S_2	heat associated with the evaporation of rain drops
T	absolute temperature
t	time
U	total horizontal wind speed
u	wind component in the x direction
U_*	friction velocity
U_g	x - component of the geostrophic wind
v	component of the wind in the y direction
V_r	terminal velocity of rain drops
ω	vertical velocity in z–coordinates
z_o	roughness parameter
σ	height in a terrain–following coordinate system
$\dot{\sigma}$	vertical velocity in the σ - system
Θ	potential temperature
Θ_*	friction potential temperature
ρ_s	density of air (standard atmosphere)
φ	$= c_p(p/P_o)^k$ (Exner's function of pressure)
φ_H	value of φ at the top of the model
ϵ	.622 (ratio of the molecular weight of water and dry air)
Δx	horizontal grid distance

REFERENCES

Bhumralkar, C. M., 1973. An observational and theoretical study of atmospheric flow over a heated island: Part II. *Mon. Wea. Rev.*, **101**, 731-745.

Burpee, R. W. and L. N. Lahiff, 1984. Area–averaged rainfall variations on sea breeze days in South Florida. *Mon. Wea. Rev.*, **112**, 520-534.

Crow, L. W. and G. Cobb, 1962. Life cycle of tropical cumulus ins Southwestern Panama. Final Report. Contract No. NSF C 184, National Science Fundation.

Estoque, M. A. and C. M. Bhumralkar, 1969. Flow over a localized heat source. *Mon. Wea. Rev.*, **97**, 850-859.

Estoque, M. A., J. Gross and H. W. Lai, 1976. A lake breeze over Southern Lake Ontario. *Mon. Wea. Rev.*, **104**, 386-396.

Kessler, E., 1969. On the Distribution of Water Substances in Atmospheric Circulation. *Meteor. Monogr.* No. 32, Amor. Meteor. Soc., Boston, Mass., 84 pp.

Lorenzetti, J. A. and J. W. Wang, 1986. On the use of wave absorbing layers in the treatment of open boundaries in numerical coastal circulation models. *Appl. Math. Model.*, **10**, 339-345.

Murray, F. W. and L. R. Koenig, 1972. Numerical experiments on the relation between microphysics and dynamics of cumulus convection. *Mon. Wea. Rev.*, **100**, 717-732.

Houze, J. A., S. G. Geotis, F. D. Marks, Jr. and A. K. West, 1981. Winter monsoon convection in the vicinity of North Borneo. Part II: Structure and time variation of clouds and precipitation. *Mon. Wea. Rev.*, **109**, 1595-1614.